

AperTO - Archivio Istituzionale Open Access dell'Università di Torino

**Virtual reality framework for editing and exploring medial axis representations of nanometric scale neural structures**

**This is the author's manuscript**

*Original Citation:*

*Availability:*

This version is available <http://hdl.handle.net/2318/1742719> since 2020-07-01T14:22:29Z

*Published version:*

DOI:10.1016/j.cag.2020.05.024

*Terms of use:*

Open Access

Anyone can freely access the full text of works made available as "Open Access". Works made available under a Creative Commons license can be used according to the terms and conditions of said license. Use of all other works requires consent of the right holder (author or publisher) if not exempted from copyright protection by the applicable law.

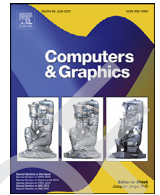
(Article begins on next page)



ELSEVIER

Contents lists available at ScienceDirect

Computers &amp; Graphics

journal homepage: [www.elsevier.com/locate/cag](http://www.elsevier.com/locate/cag)

Special Section on STAG 2019

## Virtual reality framework for editing and exploring medial axis representations of nanometric scale neural structures

Daniya Boges<sup>a</sup>, Marco Agus<sup>b,\*</sup>, Ronell Sicat<sup>c</sup>, Pierre J. Magistretti<sup>a</sup>, Markus Hadwiger<sup>c</sup>, Corrado Cali<sup>d</sup>

<sup>a</sup> Biological and Environmental Science and Engineering Division, King Abdullah University of Science and Technology, Thuwal, 23955-6900, Saudi Arabia

<sup>b</sup> Visual Computing Group, Center for Advanced Studies, Research and Development in Sardinia (CRS4), Cagliari, Italy

<sup>c</sup> Visual Computing Center, King Abdullah University of Science and Technology, Thuwal, 23955-6900, Saudi Arabia

<sup>d</sup> Department of Neuroscience "Rita Levi Montalcini", Neuroscience Institute "Cavalieri Ottolenghi", University of Turin, Turin 10043, Italy

### ARTICLE INFO

#### Article history:

Received 14 February 2020

Revised 21 April 2020

Accepted 12 May 2020

Available online xxx

#### Keywords:

Ultrastructural analysis

Medial axis representation

Immersive environments

Virtual reality in neuroscience

### ABSTRACT

We present a novel virtual reality (VR) based framework for the exploratory analysis of nanoscale 3D reconstructions of cellular structures acquired from rodent brain samples through serial electron microscopy. The system is specifically targeted on medial axis representations (skeletons) of branched and tubular structures of cellular shapes, and it is designed for providing to domain scientists: i) effective and fast semi-automatic interfaces for tracing skeletons directly on surface-based representations of cells and structures, ii) fast tools for proofreading, i.e., correcting and editing of semi-automatically constructed skeleton representations, and iii) natural methods for interactive exploration, i.e., measuring, comparing, and analyzing geometric features related to cellular structures based on medial axis representations. Neuroscientists currently use the system for performing morphology studies on sparse reconstructions of glial cells and neurons extracted from a sample of the somatosensory cortex of a juvenile rat. The framework runs in a standard PC and has been tested on two different display and interaction setups: PC-tethered stereoscopic head-mounted display (HMD) with 3D controllers and tracking sensors, and a large display wall with a standard gamepad controller. We report on a user study that we carried out for analyzing user performance on different tasks using these two setups.

© 2020 The Author(s). Published by Elsevier Ltd.

This is an open access article under the CC BY-NC-ND license.

(<http://creativecommons.org/licenses/by-nc-nd/4.0/>)

### 1. Introduction

The brain cells, together with their processes, are complex three-dimensional structures, and improving the visual understanding of the relationships between morphological features and functional aspects of these cells is of primary importance to neuroscientists. The recent progress in digital acquisition and analysis of biological samples, e.g., brain tissues, is offering unprecedented possibilities of insights for neuroscientists. For instance, automated serial section electron microscopy (3DEM) provides electron micrographs that can reach a resolution of a nanometer per pixel, therefore revealing features ranging from full structural cellular details such as axons, dendrites, and synapses (the so called "neuropil"), to smaller intracellular organelles like synaptic vesicles. However,

neuroscientists still require effective tools and applications to handle this large and complex data. Morphology data at nanoscale resolution provide domain scientists fundamental information for understanding neural processes and interaction between cellular structures [1]. Quantifications have particular relevance when extracted data are used to infer parameters allowing mathematical modelization of biological processes [2,3]. Furthermore, the challenge of making qualitative and quantitative assessments of complex and visually occluded individual cellular structures, or groups of them, is beginning to attract neuroscientists towards the use of immersive visualization paradigms. Hence, during recent years, various laboratories pioneered the use of virtual reality (VR) in supporting electron microscopy (EM) structural analysis [4–6]. However, previous pipelines were engineered around the need of exploratory analysis of brain structures for specific morphology studies [4], or neuroenergetics investigations [5,7]. More recently, the need for more efficient extraction of features of branch-based whole cell structures, either for quantification and classification

\* Corresponding author.

E-mail addresses: [magus@hbku.edu.qa](mailto:magus@hbku.edu.qa), [magus@crs4.it](mailto:magus@crs4.it) (M. Agus), [corrado.cali@unito.it](mailto:corrado.cali@unito.it) (C. Cali).

<https://doi.org/10.1016/j.cag.2020.05.024>

0097-8493/© 2020 The Author(s). Published by Elsevier Ltd. This is an open access article under the CC BY-NC-ND license.

(<http://creativecommons.org/licenses/by-nc-nd/4.0/>)

32 purposes [8], has emerged. Especially neurons, but also glia, can  
33 be adequately schematized through skeleton representations, and  
34 nowadays, various laboratories are investing important resources  
35 on creating faithful and smooth medial axis representations of  
36 brain cells. These skeleton representations can be used for various  
37 kinds of novel visual and statistical analysis. To this end, time  
38 consuming image-based manual tools [9–11] are commonly used  
39 for tracing neural processes on confocal images. More complicated  
40 automatic methods for recovering medial axis representations on  
41 nanometric scale electron microscopy stacks exist but are still in  
42 their infancy [12] and not yet routinely used for processing brain  
43 cells.

44 In this paper, we present a novel VR-based framework targeted  
45 on creating, proofreading, and exploration of skeleton-based rep-  
46 resentations of nanoscale brain cells surface reconstructions. The  
47 system integrates the following components:

- 48 • Fast servo-assisted semi-automatic methods for creating skele-  
49 tons of complex brain cellular reconstructions.
- 50 • Tools for proof-reading (checking, correcting, comparing) me-  
51 dial axis representations.
- 52 • Exploration tools, e.g., for performing geometric measurements  
53 and statistical computations related to cellular structures and  
54 their skeletal representations.

55 The system is currently used by expert domain scientists for  
56 analysis of various cells reconstructed from the somatosensory cor-  
57 tex of a juvenile rat [1]. We report on a preliminary subjective  
58 evaluation of the immersive environment performed by domain  
59 experts during creation and proofreading of complex medial axis  
60 representations, as well as during analysis of organelles distribu-  
61 tions. This paper is an extended version of the proceeding contri-  
62 bution presented at Smart Tools and Applications for Graphics con-  
63 ference [13]. We provide here a more thorough exposition, together  
64 with a more effective external semiautomatic tracing tool for edit-  
65 ing medial axis branches. Moreover, we extended the framework  
66 to work in a monocular setup with a large scale display wall, and  
67 we carried out a user study for evaluating the performances of the  
68 system for creating and editing skeleton representations, either in  
69 the monocular display wall setup and in the stereoscopic HMD-  
70 based virtual reality setup. To our knowledge, this is the first inter-  
71 active system targeted to the creation, proof-reading and analysis  
72 of skeleton-based representation of cellular structures, and the pre-  
73 liminary reports of usage by expert and novice users provided us  
74 promising indications that these kind of systems can positively ef-  
75 fect the way ultrastructural analysis is carried out in neuroscience  
76 domain.

## 77 2. Related work

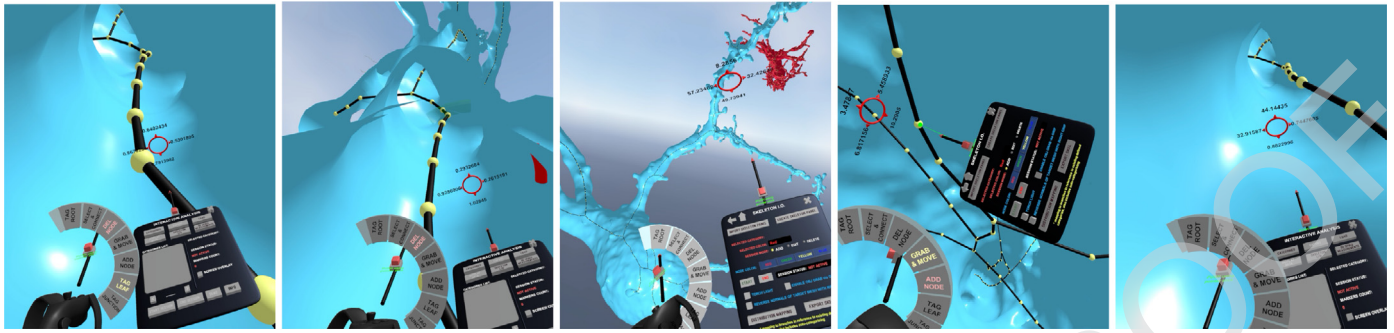
78 Our work deals with the application of virtual reality (VR) tech-  
79 nologies to neuroscience investigations coupled with the compu-  
80 tation of medial axis representations of highly detailed branched  
81 cellular brain structures. In the following, we discuss the previous  
82 work mostly related to our contribution.

83 *Virtual reality in neuroscience.* Due to the ubiquity of desktop  
84 systems, most commonly used visual analysis tools in neuroscience  
85 are designed as desktop applications [14,15]. However, more re-  
86 cently, there is general consensus that the use of stereoscopic tech-  
87 niques, e.g., in VR systems, can provide a more immersive way to  
88 explore brain imaging data [16], and that the increased dimension-  
89 ality provided by stereoscopy is beneficial for understanding depth  
90 in the displayed scenery [17,18]. With respect to immersiveness,  
91 the effect of stereoscopy has been previously evaluated in the con-  
92 text of visual analysis of volume data, particularly for semitrans-  
93 parent volume rendering [19,20], isosurfaces [21], confocal volume

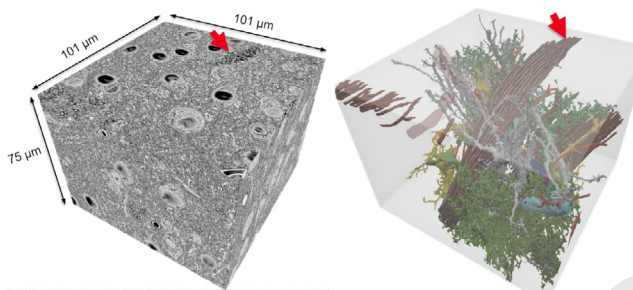
images [22], and for interactive graph analysis [16,17,23]. Success-  
ful examples of applying VR technologies to neuroscience investi-  
gations include analysis of glycogen distribution related to neural  
morphologies [4], systems for exploring connectomes [24], systems  
for tracing neurons in microscope scans of primates' visual cor-  
tex [6], and the use of heat maps for representing absorption prob-  
abilities on nanoscale surface reconstructions [5]. Very recently Xu  
et al. [25] introduced TempoCave, a system for analyzing dynamic  
brain networks by exploring activity patterns in different regions  
in the brain, computed by processing raw data retrieved from func-  
tional magnetic resonance imaging (fMRI) scans [25]. In this work,  
we describe an immersive environment for performing shape anal-  
ysis that is mainly targeted on skeleton representations of nano-  
metric reconstructions. To our knowledge, it is the first application  
of a VR environment towards morphological analysis of medial axis  
representations, particularly of brain cells.

*Skeleton-based representation of surface meshes.* Medial axis rep-  
resentations or skeletons can be considered descriptors which  
jointly describe the geometry, topology, and symmetry proper-  
ties of a shape in a compact and intuitive way, providing a  
means to capture the essence of a 3D shape [12]. Automatically  
or semi-automatically producing accurate skeleton representations  
is a challenging task. During the last decades, many techniques  
have been proposed, particularly by the computational geometry  
community, for different kinds of 3D models. For a comprehen-  
sive discussion of the recent methods for creating 3D medial axis  
representations, we refer the readers to state-of-the-art reports by  
Tagliasacchi et al. [12], and by Sobiecki et al. [26]. In general, there  
is a huge collection of methods to obtain 3D skeletons, which  
can be classified according to the input representation: mesh-  
based [27–30] and voxel-based representations [31]. Since our sys-  
tem is focused on surface representations, we will mostly consider  
methods that use meshes, even if our system can be considered  
independent from the method used for obtaining the medial axis  
representation of the morphology considered. The system has been  
designed to import skeleton representations coming from differ-  
ent automatic frameworks: for our initial analysis, we considered  
the Mean Curvature Skeleton (MCS) algorithm [27], and the Center  
Line Tree method [32], which are implemented in the Avizo [33]  
framework.

*Medial axis representations in neuroscience.* Since medial axis  
representations provide an adequate and convenient description  
for branched structures, recently, neuroscientists started exploiting  
them for representing complicated cellular structures, especially  
neurons. To this end, they derived specific metrics for comparing  
branched structures, i.e., trees, based on geometrical and topolog-  
ical features [34–36]. These metrics are then used for investigat-  
ing differences and analogies between morphologies or in gen-  
eral for performing identification and classification [37–39]. Fol-  
lowing this philosophy, recently Kanari et al. [40] developed a  
classification framework for neurons completely based on skele-  
tons, which is based on specific topological representations, called  
persistence diagrams. The framework has been successfully used  
for objective morphological classification of neocortical pyramidal  
cells [8]. It has also been integrated into a more general collabora-  
tive framework for the analysis and visualization of neuronal mor-  
phology skeletons reconstructed from microscopy stacks [41]. Our  
proposed immersive environment addresses similar needs, and it  
is customized for the proofreading and analysis of skeletons of dif-  
ferent cells, while leveraging the benefits of a VR system. We be-  
lieve that 3D branched structures derived by brain cell morphol-  
ogies can be more effectively analyzed by leveraging cues provided  
by stereoscopy and full immersion which are well suited for 3D  
scenes. Our framework is general and customizable, and it can be  
extended to integrate other geometric representations and visual  
encodings.



**Fig. 1.** Our proposed virtual environment enables neuroscientists to immersively create, proofread, and explore medial axis representations or skeletons of nanoscale reconstructions of brain cells. In the example scenario above, skeletons are represented as connected nodes (yellow spheres) and edges (black cylinders), while brain cells are depicted as shaded surfaces (using a light blue color in this example). (For interpretation of the references to color in this figure legend, the reader is referred to the web version of this article.)



**Fig. 2. Data preparation.** Left: we tested the proposed immersive system on models reconstructed from an image stack acquired by serial electron microscopy of a sample from a juvenile rat's somatosensory cortex. Right: sparse reconstruction provides high resolution surface representation of full cellular morphologies.

### 160 3. Application domain: Morphology analysis in neuroscience

161 Before detailing the proposed immersive environment, we first  
162 provide a brief description of our particular application domain  
163 in neuroscience: the ultrastructural investigation of brain cellular  
164 morphologies at nanometric scale.

165 **Ultrastructural analysis.** Neuroscientists often perform ultra-  
166 structural analysis of brains samples through ex-vivo digital ac-  
167 quisition of very small brain portions. To this end, they use high  
168 resolution electron microscopy systems equipped with high pre-  
169 cision cutters [42]. Through this methodology, domain scientists  
170 get 3D 8bit image stacks containing cellular membranes at nano-  
171 metric resolution (see Fig. 2 left). These datasets allow them to  
172 visually individuate and annotate cellular and molecular features,  
173 such as compounds, synapses, and organelles like mitochondria,  
174 vesicles and endoplasmatic reticulum (ER). Nowadays, EM imaging  
175 technique is becoming increasingly popular in the field of connec-  
176 tomics, since it enables accurate reconstructions of the connections  
177 between neurons [43].

178 **Processing pipeline.** Given a 3D stack of images acquired by  
179 an electron microscope (Fig. 2 left), neuroscientists need to pass  
180 through different processing tasks in order to extract relevant 3D  
181 shape representations of cellular structures, in form of surface  
182 meshes (Fig. 2 right), that can be used for statistical computations,  
183 simulation, or rendering. The processing pipeline consists of carry-  
184 ing out dense or sparse reconstructions, by using manual, semi-  
185 automatic or automatic tools, which label the image pixels in the  
186 stack, i.e., assigning them with a unique object identifier for the  
187 various structures of interest, such as neural axons, dendrites, or-  
188 ganelles, nuclear envelopes, etc. In this work, we used a hybrid  
189 two-step pipeline [44], composed by:

- A rough automatic segmentation performed offline through the iLastik tool [45], for finding the gross features and processes of a cell.
- A manual proofreading phase, performed through the TrackEm2 tool [46], for specifying exact object boundaries and finer details.

**Morphology features.** Once the various cells and sub-parts are labelled on a per-pixel level in the image stack, neuroscientists perform various ultrastructural analyses by studying the morphology of the following biological structures (Fig. 2 right):

- **Neurons:** composed of *axons* and *dendrites*, which are the terminals respectively sending and receiving electric signals through *boutons* and *spines*. Boutons and spines are linked and form *synapses*.
- **Glial cells:** neuroscientists mainly focus on *astrocytes*, which are metabolically involved in feeding neurons, *microglia*, which are the main form of active immune defense in the central nervous system by acting as macrophages, and *oligodendrocytes*, which produce the myelin sheath insulating neuronal axons.
- **Organelles:** domain scientists mainly focus on *mitochondria* and *endoplasmatic reticulum*, which are contained in axons, dendrites, and glial cells. They contain the machinery for chemical transformations.

Neuroscientists are interested in studying the relationships between the aforementioned structures, and perform geometric analysis for recovering parameters to be used for simulation purposes or for classification [40,47].

**Medial axis representations.** Most of the considered cells have complicated branching structures, which are very difficult to analyze using standard mesh representations (see Fig. 2 right). To this end, skeleton representations provide an effective tool for describing them and classifying the various branches, according to the size and the branching level, starting from the soma. For this reason, neuroscientists are increasingly focusing on technologies that can support them in recovering accurate skeletal representations [8,35].

### 4. System overview

The proposed system is a standard 3D framework customized to be used with a stereoscopic HMD-based setup using room scale tracking technology (VR), or with a large screen display for collaborative sessions. In VR, the system allows the user to interact with a 3D environment through two motion-tracked hand-held controllers, i.e., by pointing/selecting objects, or selecting motions through menus. When working with the display wall, a generic

**Table 1**  
Notations/formats used for skeleton data.

| Algorithm/Tool               | Notation/ File Format  | Data Type                                   |
|------------------------------|--|---|
| Centerline Tree (Avizo)      | [ Point ID, Thickness, X Coord, Y Coord, Z Coord ]/.CSV<br>[ Segment ID, Node ID1, Node ID2, Point IDs List ]/.CSV | Points (file1)<br>Branches(file2)           |
| Mean Curvature Flow          | [ x, y,z ] / .txt<br>[ NodeID1, NodeID2 ]/.txt   | Points (file1)<br>Branches (file2)          |
| Simple Neurite Tracer (Fiji) | [ Sum of points(n), X, Y, Z, Xn,Yn,Zn ]/.txt<br>[ NodeID, Cell Type, X, Y, Z, radius, ParentID ]/.SWC              | Points and Branches<br>Points with Branches |

gamepad controller can be used for input. The framework was developed on top of the Unity game engine.

**Scene representation and rendering.** The immersive environment provides real-time exploration of scenes composed of surface representations of brain cells and schematic representations of the associated medial axes or skeletons. The level of transparency of surfaces can be interactively controlled in a way to provide context for skeleton exploration. Since the system is also designed for providing endoscopic analysis of cellular processes, a torch tool is provided for shading mesh walls and dark corners during exploration. The tool is attached to one of the manipulators and can be easily used to illuminate dark areas. Basic 3D manipulation options are provided, e.g., object scaling and placement, as well as material and color assignment. Moreover, users can flip the mesh normals, in a way to have a more convenient way of examining the inner/outer mesh surfaces. With respect to skeletons, the system uses three different representations:

- **sprite-based:** 2D line segments/ribbons represent the whole skeleton geometry (implemented using Unity line renderer module);
- **Node-based:** only spheres represent skeleton nodes; depending on the skeleton data, the system can utilize only primary nodes to provide a rough representation of skeletons.
- **Complete:** skeleton nodes are represented by spheres while skeleton edges are represented by cylinders.

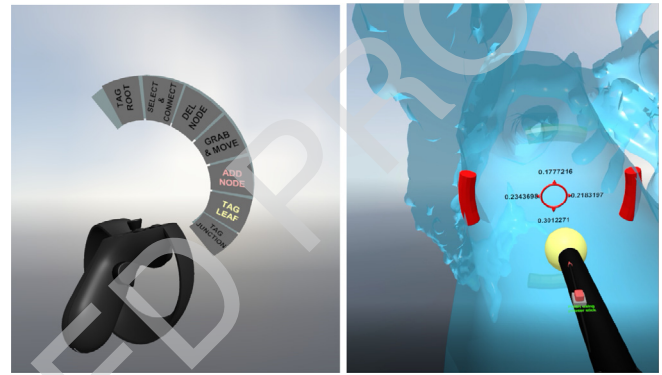
**Main features.** After loading the cellular morphology, the system enables users to operate on medial axis representations in two modes: *create mode* for creating skeletons from scratch, and *proof-read mode* for correcting/editing previously computed skeletons. In proofread mode, the system requires that previously computed medial axes respect specific notations represented in Table 1. This notation is valid for most graph representations and is widely used by many graph processing software. Specifically, in this paper, we focused on skeletons computed through three methods:

- An automatic volume-based method [32], implemented in the Avizo framework [33] - it uses connected components for graphs, combining a union-find and a recursive algorithm.
- An automatic mesh-based method [27] - it uses iterative contraction through mean curvature flow evolution.
- A manual image-based tracer implemented in the Fiji system [10].

The system provides support for importing and exporting standard skeleton file formats that are compatible with the previously mentioned systems. It can also be easily extended to support other formats/notations.

## 5. Interactive tools

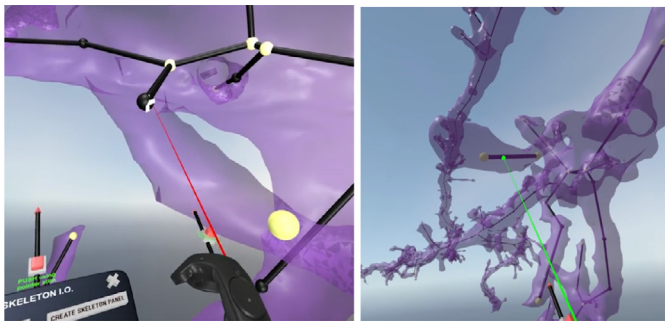
The proposed system provides interactive tools for editing/manipulating medial axis representations. We describe available interactions using 3D controllers for VR as well as for gamepad controllers for the display wall. We tried to keep most interactions similar for the two controllers in order to reduce the



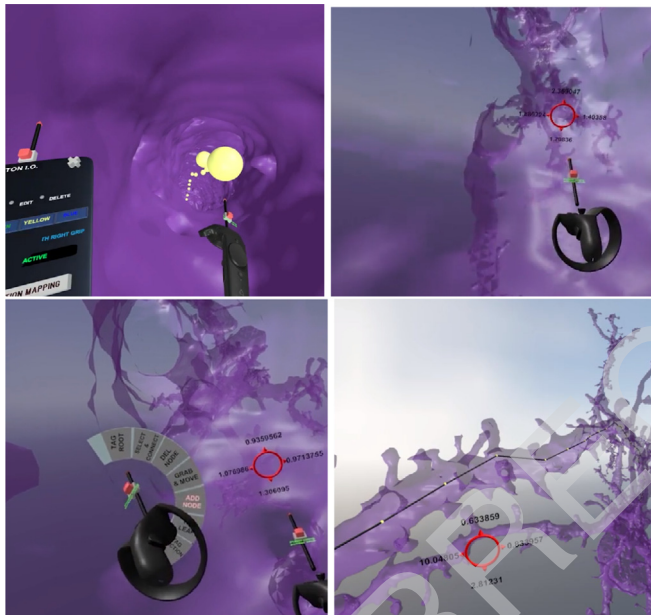
**Fig. 3. Interactive tools.** Left: an arch-shaped menu attached to the left controller allows users to select interaction mode with skeletons. Right: a stabilizer servo-assisted tool (in red) guides users through the process of skeleton branch tracing. (For interpretation of the references to color in this figure legend, the reader is referred to the web version of this article.)

effort for users in terms of switching between the two if necessary. In the following, we discuss interactions based on 3D controllers but the same applies to a gamepad with the trigger button corresponding to gamepad buttons with pre-mapped functions, and 3D pointing corresponding to using the gamepad arrow and analog buttons to move the camera and the pointer. The core interactions are summarized in 7 options laid out in an arch-shaped menu (see Fig. 3 left), attached to the left 3D controller. The user can choose one of the options by first rotating his/her wrist between 0° and 180°, and then, once settled on an option, pressing the trigger buttons to select. The options provided by the system are the following:

- **Add Node:** using the trigger button, the user can create a node in 3D space. This process can be fully manual or controlled by a servo-assisted stabilizer. Upon creation, the system automatically pairs up nodes with each other and connects them with an edge, hence, creating a single connected path.
- **Grab and Move:** as part of the proofreading/editing process, nodes can be moved anywhere simply by grabbing them and moving them. This can be achieved thru a combination of an action grab initiated by pressing and holding of the controller's *grip* button while touching the surface of the target node.
- **Select and Connect:** using a combination of point and trigger click, the user can select two nodes subsequently and the system creates an edge connection between them (see Fig. 4 left).
- **Delete Skeleton Element:** the system allows the right controller to shoot a laser pointer by pressing on the controller touch pad. The user can then delete nodes and edges by pointing at a valid skeleton unit object followed by a trigger button click (see Fig. 4 right).
- **Tag Root, Junction, and Leaf:** a similar action of point and trigger at a specified node will save it in its corresponding skeleton file as one of these values: 0=Root, 1=Internal, 2=Leaf, 3=Junction. Tagging a node with "Leaf", "Junction", or "Root"



**Fig. 4. Skeleton editing.** Our system provides effective tools for rapid editing of skeleton branches. Left: adding connection between nodes. Right: removing a wrong edge from a skeleton branch.



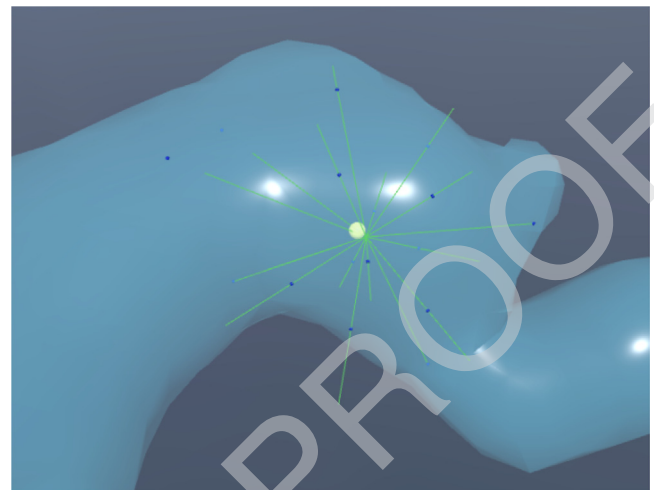
**Fig. 5. Skeleton creation.** We propose a semiautomatic and guided method for creating skeletons, based on endoscopic exploration of cell branches, and using a servo-assisted stabilizer.

marks it with a special color material and finalizes the current path as a single branch.

- **Undo:** an action that saves users the troubles of having to delete a mistake node manually, and instead, they can revert to multiple steps back during the skeleton creation process.

*Path stabilizer: tunnel metaphor.* The system provides a semi-automatic method for creating skeleton branches through one of the VR input controllers. This method is built around a visual user guide, that operates as reference when tracing the tunnel-like cellular processes through endoscopic navigation. During the exploration of the process, a path stabilizer transparently and automatically places skeleton nodes in the middle of the process section. The automatic node position computation is performed by shooting straight rays onto a number of radial directions, and computing the average distance to the surrounding wall boundaries. This simple but effective method provides a way to rapidly trace main cellular processes, and create fully controlled skeleton representations. In current implementation we use 16 rays for computing the average distance.

*Path stabilizer: tracing metaphor.* In order to speed up the tracing process of long branches exhibiting low curvature, like it happens for some neural dendrites and axons, we introduced a semi-automatic external tracing metaphor. With this tool, user is able



**Fig. 6. External tracing.** Users can trace branches through external 3D pointing, since a semiautomatic algorithm computes running barycenters through multiple iterative ray casting.

to follow the path of the specific through 3D pointing, while the system uses ray casting for intersecting the branch, and, starting from the ray, an iterative approach shoots different rays similarly to the previously described tunnel metaphor. In order to accelerate the computation of nearest neighbors, we use a KD-tree data structure. The running barycenters of the different ray intersections are added as nodes in the current skeleton branch. Even in this case, in current implementation we use 16 rays for computing the running barycenter. This method proved to be very fast and effective for processes not exhibiting sharp features and bumps (see Section 7). Fig. 6 shows an example of the algorithm for computing a node.

## 6. Setup and dataset

Our proposed immersive system is used by neuroscientists for performing real-time creation, proofreading/editing, and exploration of brain cell reconstructions based on medial axis representations.

*Implementation details.* The immersive system has been developed and deployed using the Unity game engine (version 5.6.3, via C# scripting). For VR, it uses SteamVR and the VRTK software packages [48], which provide smooth immersive system-user interaction as well as cross-hardware setup compatibility. In this way, the same application can be used on various VR setups, like Oculus Rift [49] or HTC Vive [50]. For computing automatic skeletons, and for other preprocessing tasks, we implemented and used C++ applications and Python scripts. In addition, we used Avizo (a commercially available data analysis/visualization software framework) for computing high-quality skeletons, and preprocessing was carried out on a workstation equipped with two CPUs of 10 cores each (see Table 2 for additional details).

*Data preparation.* For testing purposes, we considered five complex cellular structures reconstructed from a p14 rat somatosensory cortex. We selected different kinds of cells to show different levels of complexity: two neurons, two microglia, and one astrocyte [1]. The cells were reconstructed from a high-resolution EM stack with approximated size of  $100\mu\text{m} \times 100\mu\text{m} \times 76.4\mu\text{m}$  (see Fig. 2 left). The reconstruction process was performed through a semiautomatic process [44] involving customized components and public domain software like iLastik [45] and TrakEM2 [46]. The output of the reconstruction process is a series of high resolution triangular meshes representing the cellular morphologies (see Fig. 2 right). Furthermore, each cell was optimized in a way to be

**Table 2**  
Machines used for immersive environment and data preparation.

| Machine        | OS              | Task                                  | Specs  |
|----------------|-----------------|---------------------------------------|--|
| Asus ROG G703G | Windows 10 Pro- | Immersive environment                 | 32GB DDR4, Intel Core i9-8950HK 4.8GHz, Nvidia GTX 1080 8GB GDDR5X, 2X 256GB PCIE SSD + 2TB SSHD FireCuda. |
| Supermicro     | Linux CentOS 7  | Data processing and skeleton creation | 1TB memory, Intel(R) Xeon(R) Gold 6150 CPU 2.70GHz (18 Cores), Nvidia GK104GL Quadro K5000, N/A            |

watertight and without non-manifold edges and vertices, and in a way to preserve all important morphological features. To this end, we used public domain mesh processing tools like Blender [51], Meshlab [52], and Ultralizer, a geometry processing tool contained inside the suite NeuroMorphoVis [41]. For getting automatic medial axis representations of the considered morphologies, we used the Mean Curvature Skeleton algorithm [27], as well as the Centerline Tree module both available in Avizo [32]. In Table 3 we report on the cell morphologies and the associated skeleton representations. Specifically we provide visual representations of the morphologies, together with information about their shapes and sizes in terms of vertex counts, visual representations of automatic skeletons, and skeleton graph statistics (number of nodes, number of edges, and number of branches).

**Hardware setups.** We tested the VR application on a gaming laptop equipped with an Nvidia GTX 1080 8GB GDDR5X GPU. We used the laptop to drive two different display setups (see Fig. 8):

- A stereoscopic immersive Head Mounted Display (HMD) Oculus Rift S [53] with sensors embedded in a way to lower the bulkiness of the system and increase portability. The display uses a single fast-switch LCD panel with a resolution of  $2560 \times 1440$  with a refresh rate of 80 Hz, field of view of 110 degrees on a workspace of  $3.5 \text{ m} \times 3.5 \text{ m}$ ;
- A monocular collaborative large-scale display wall composed of an array of tiled  $3 \times 4$  Narrow Bezel Monitors (55") ( $7680 \times 3240$  pixels) for a total resolution of around 25 Mpixels. For the monoscopic display setup, the Oculus Rift input devices were substituted by an Xbox gamepad controller.

The two different setups provide different working environment in which the tools can be used as direct pointers for performing editing operations on the scene. The proposed interacting metaphors are general and can be adapted to different setups, using different kind of controlling devices, like touch devices or gestures [54]. According to the taxonomy presented by Mendes et al. [54], the considered setups are the following: an immersive one, with 3D controllers physically providing a direct metric control over the scene represented in a virtual workspace, and a gaming one, with gamepad controllers controlling a 2D display wall, in an indirect way. Regarding the design choices, we decided to do not use the same controllers in both setups since the oculus controllers are natively connected to a real 3D physical setup, and we believe they would not be naturally understood if coupled to a monoscopic display setup.

## 7. Results

We carried out a preliminary assessment of the system to understand how is the usability in the context of exploratory analysis of different kind of cells. We report here on two kind of eval-

uations: a subjective qualitative assessment performed by expert users on complete creation of skeleton representations of entire cells, and an user study for evaluating the performance of the system for editing tasks either in HMD-based stereoscopic setup and Wall-based monoscopic setup. Finally we report on a use case for measurement analysis on distributions of branched-like organelles.

### 7.1. Expert evaluation

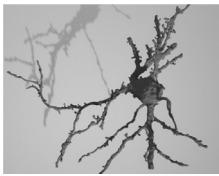


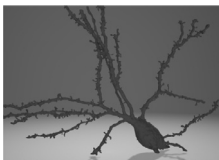





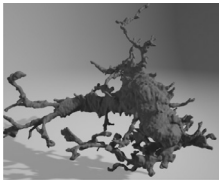


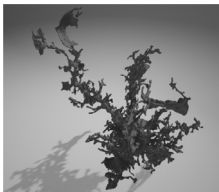


A preliminary evaluation of the system was performed by two expert neuroscientists on cells of Table 3. Domain scientists were particularly interested in obtaining accurate and clear skeletal representations to be used as descriptors of highly intricate cellular structures. In general, they want to have precise control of medial axis representations, in a way to be able to clearly separate main processes from fine details that have different biological meaning (for example dendritic shafts and spines in neurons). In this sense, most automatic systems provide "dirty" medial axis representations, thus we expected that an interactive tool helping in cleaning skeletons would receive a positive feedback. Moreover, we expected that the immersiveness provided by virtual reality could improve the creation and editing process.

**Skeleton creation from scratch.** Neuroscientists used the system for creating skeletons from scratch on two neural morphologies. In Table 4, we show statistics about the skeleton creation process, with different tracing metaphors (internal and external) and different display setups (VR-based and Wall-based). The procedure consisted of exploring the surface models in order to select the main processes, and trace the branches from inside the cells, i.e., similar to an endoscopic navigation/view. Domain scientists felt comfortable in recognizing main processes, e.g., dendrites and spines, in a way to correctly trace the medial axis of interest. Moreover, they felt quite comfortable with the path stabilizer, which reduced the number of input actions on controllers. A comparison of creation times between the two different display setups and the different tracing interfaces shows that expert users were faster when using external tracing metaphor with stereoscopic VR setup (almost 2X with respect to the worst case according timings in Table 4).

**Skeleton proofreading/editing.** Automatically computed skeletons were examined by domain scientists through the proposed system (see Fig. 7). They used the system for comparing skeletons automatically computed through Mean Curvature Flow (MCS [27]), and Centerline Tree (CLT [32]). They concluded that both the methods considered were able to cover all the morphology features of interest. However, skeletons produced by CLT appeared to be too highly detailed, with a number of wrongly assigned branches as well as disconnected parts. Table 5 shows the difference in the total number of branches, nodes and edges for each algorithm for all five cells. In general, domain scientists found that skeletons produced by MCS algorithm contained a lower number of artifacts. For this reason, in all considered cases, they preferred to perform editing and cleaning on skeletons computed through MCS algorithm. To this end, they carried out a series of checks depending on the type of cell, and on the biological significance of the various features:

- Identify main branches by tagging their nodes as either leaf, end of branch, or internal nodes. The system identifies all node types based on the degree of each one in the graph tree. However, some needs to be adjusted based on the cell's biological features. Using the VR interactive menu, the user points at a node with the VR controller's laser pointer and then clicks on the trigger button to tag it. The node's color material will switch color indicating that it is saved in the system based on the tagging feature. In the case of neurons, the main branches would be all dendrites, excluding any other features e.g., spines.



**Table 3**  
**Morphologies and Mean Curvature Skeletons (MCS) of 5 biological cells.** Cells are computed automatically through [27] and proofread and cleaned through our Virtual Reality system. Together with pictorial representations, we report on cell sizes, total times for proofreading and cleaning, and skeleton statistics.

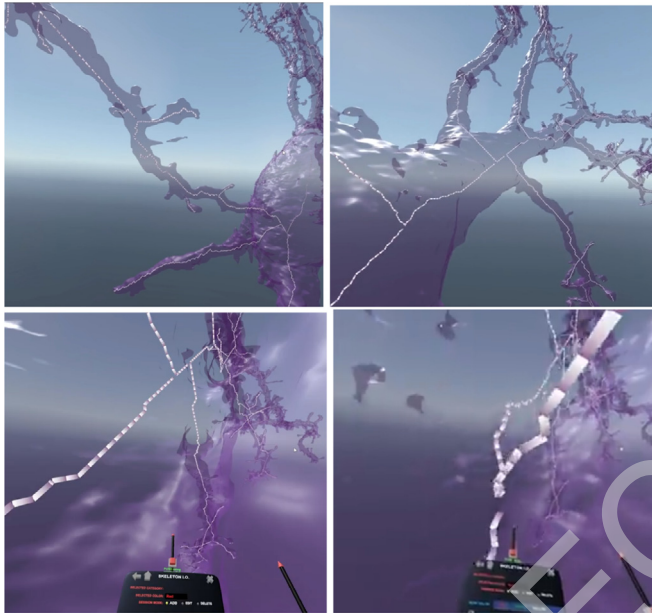
| Name       | Picture   | Vertices | Time  | Before cleaning  | Nodes-Edges-Branch | After cleaning  | Nodes-Edges-Branch |
|------------|---|----------|-------|--|--------------------|---|--------------------|
| Neuron1    |    | 49,628   | 10.00 |    | 1569  1573  201    |    | 1318  1321  25     |
| Neuron2    |    | 78,215   | 15.28 |    | 1,619  1,629  357  |    | 1215  1223  20     |
| Microglia1 |    | 48,015   | 09.00 |    | 1,463  1,479  165  |    | 1443  1456  62     |
| Microglia2 |   | 125,532  | 13.53 |   | 2,105  2,122  260  |   | 2060  2077  111    |
| Astrocyte  |  | 211,004  | 25.16 |  | 4,055  4,137  854  |  | 3906  3983  296    |

Please cite this article as: D. Boges, M. Agus and R. Sicat et al., Virtual reality framework for editing and exploring medial axis representations of nanometric scale neural structures, Computers & Graphics, <https://doi.org/10.1016/j.cag.2020.05.024>



**Table 4**  
Statistics on skeletons generated semi-automatically from scratch for Neuron1 and Neuron2 morphologies.

| Cell Name | Skeleton  | Time Stereo Int | Time Stereo Ext | Time Mono Int | Time Mono Ext | Nodes  Edges  Branches |
|-----------|---|-----------------|-----------------|---------------|---------------|------------------------|
| Neuron1   |  | 25:13           | 14:24           | 29:55         | 25:28         | 481  480  25           |
| Neuron2   |  | 30:50           | 14:35           | 22:54         | 24:11         | 629  628  20           |



**Fig. 7. Skeleton proofreading.** Our system enables domain scientists to perform effective proofreading of skeletons by using endoscopic and external metaphors.

**Table 5**  
Neuron1 and Neuron2 skeleton properties as generated via Mean Curvature Skeleton (MCS) and Centerline Tree (CLT) algorithms.

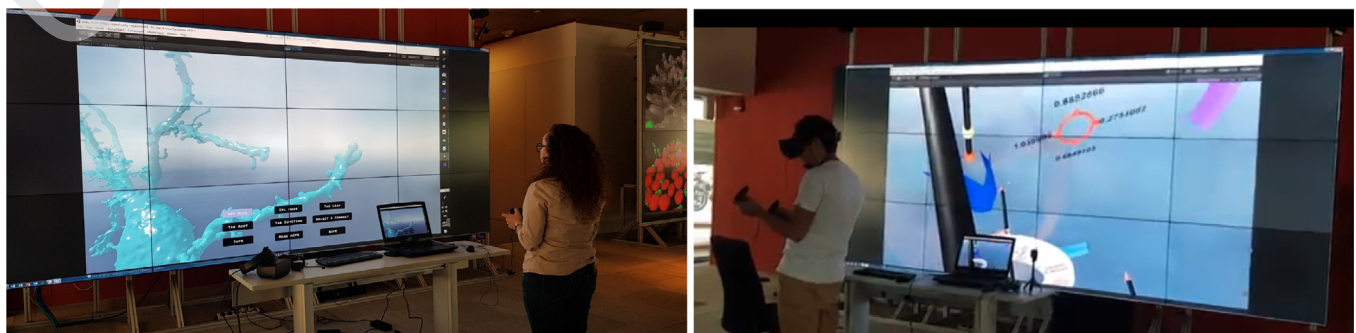
| Cell Name | Algorithm | Nodes Edges Branches |
|-----------|-----------|----------------------|
| Neuron1   | MCS       | 1569   1573   201    |
|           | CLT       | 7719   7328   361    |
| Neuron2   | MCS       | 1619   1629   357    |
|           | CLT       | 9655   9530   516    |

- In the case of highly-detailed skeletons, one would encounter duplicate nodes and edges, disconnected parts, loops, and out of track skeletonization. Neuroscientists tried to delete all defects through an iterative manual process.

- The soma area should be clear from any branching so neuroscientists “cleaned” these parts by deleting all branches and merging them into one.

In last two columns of Table 3, we show the proofreading outputs for all the considered cells. In general, domain scientists found the proofreading task comfortable and accurate, and they particularly appreciated the immersiveness of the system for checking features and recognizing defects. For comparison, we asked expert neuroscientists to perform skeleton cleaning by using the external tracing metaphor together with the wall display setup: timings recorded for Neuron1 (27 m58 s) and for Neuron2 (46 m10 s) provided us evidence that the monoscopic setup associated to the external interface is not comfortable for cleaning skeletons.

*Discussion.* In general, one of the drawbacks of dealing with an immersive environment on long sessions (20 min and more), is the symptoms of cybersickness and fatigue. This happened also for our system, and, during the sessions, users needed to take breaks every 15 min when performing each task. To this end, the system allows for multiple saves across sessions, and the user can retrieve the file anytime and continue where he/she last stopped. From this point of view, users liked the display wall setup in case of cyber-fatigue, since they could sit, and rest while still working on the task. As general impression, the system was considered very useful for both proofreading/cleaning pre-exported skeletons, as well as for creating skeletons from scratch. In particular, neuroscientists trained in neurite tracing found very effective how the tool automatically provides a centerline, without the hassle of having to place it manually. Although the process of creating skeletons from scratch in VR can be time-consuming, automatic tools can make a lot of mistakes, and the time saved on the manual tracing would be lost on the proofreading anyways. This largely balanced the costs/benefits of the two approaches. Several factors contributed to make the creation process time consuming, mainly technical. One factor involves the order of tracing the various branches. Specifically, in some cases, users started tracing from the soma and proceeded towards the tips, while in other cases they made the opposite choice, by starting from the tip of the most extended branch and tracing towards the soma. We also experienced that another



**Fig. 8. Display setup for user study.** We evaluated the system performance under different display conditions: large scale monoscopic display (left), and head mounted stereoscopic display (right).

535 source of error was the path-stabilizer, in cases where the user  
 536 happened to release a node at a bifurcation spot. Since the path-  
 537 stabilizer is based on the concept of ray-casting, users needed to  
 538 take care of correctly keeping the VR controller within the walls of  
 539 the cellular structure. Issues with the stabilizer were experienced  
 540 also in cases when the cell's main branch has too many spines  
 541 within close distance to each other. In such situations, neuroscien-  
 542 tists sometimes preferred to disable the stabilizer and operate on a  
 543 full-manual mode. In general, we noticed that most creation issues  
 544 were alleviated as users gained experience with the system, and  
 545 we think that performance should dramatically improve once users  
 546 repeat the process for many cells, i.e., after further training and  
 547 experience. From the quality point of view, neuroscientists were  
 548 satisfied with skeletons generated from scratch in VR, since they  
 549 appeared well-structured and represented precisely the biological  
 550 structure of the cells, tailored accordingly to their experience  
 551 and knowledge about cell morphology. Regarding the proofreading  
 552 task, domain scientists performed very well in checking and  
 553 editing all five skeletons. They experienced some problems only  
 554 with the Astrocyte, which took around 25 minutes to be proofread  
 555 and edited. This is due to the fact that astrocytes have very com-  
 556 plicated branched structures (see Table 3), where main processes  
 557 are very difficult to recognize at first sight even for expert domain  
 558 scientists.

## 559 7.2. User study

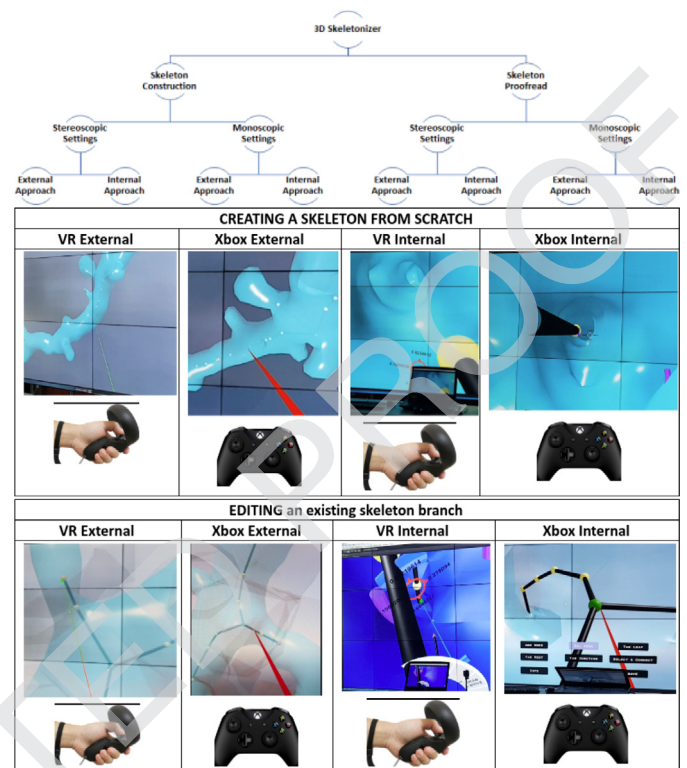
560 The use of Virtual Reality in Neuroscience is still at its early  
 561 stages [5,55], therefore the user studies for evaluating the perfor-  
 562 mance of Virtual Environments for editing tasks are currently de-  
 563 signed almost from scratch, because of the lack of standardized  
 564 guidelines [56]. In our case, we aimed to assess the performance  
 565 of the system for creating and modifying skeleton representations  
 566 of brain cells. To this end, we involved 12 users with different  
 567 level of experience, and we asked them to perform specific tasks  
 568 under different conditions. We measured times and accuracy, and  
 569 we assessed the fatigue and comfort through NASA-TLX question-  
 570 naire [57]. In the following we detail the design of the user study  
 571 and the outcomes of evaluation. The main goal of the study was  
 572 to evaluate the effects of HMD and wall display on system per-  
 573 formance, and whether users felt more comfortable with external  
 574 or internal tracing metaphor for editing purposes (see Fig. 8). The  
 575 study took place in the visualization lab facility of King Abdullah  
 576 University of Science and Technology, and in the department of  
 577 Anatomy at University of Turin.

578 *Design and protocol.* Subjects were asked to perform various par-  
 579 tial tasks on the system, using HMD or Wall display, and using in-  
 580 ternal or external metaphor for editing operations. Specifically, af-  
 581 ter a period for training and getting comfortable with the various  
 582 setups and tools, we asked users to edit the skeleton of a brain cell  
 583 in the following way:

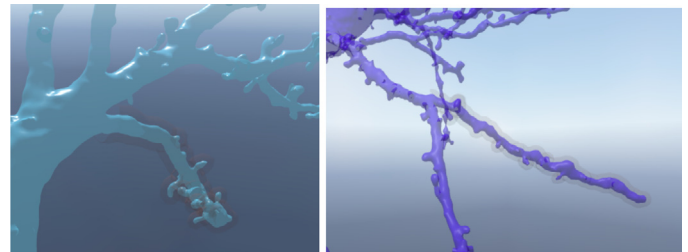
- 584 • Trace a full branch.
- 585 • Correct a branch by removing nodes and links.

586 The branches to be traced were chosen randomly from two  
 587 long dendritic processes of Neuron1 and Neuron2 (see Fig. 10). Be-  
 588 fore each task, the user was shown how the task is performed  
 589 and how the joystick controls are being operated. They were given  
 590 a few minutes to practice the task until they were comfortable  
 591 enough to go ahead and start their mission. Water and refresh-  
 592 ments were offered at all times during the study. Equipment were  
 593 wiped and cleaned thoroughly with antibacterial wipes after each  
 594 use.

595 The two tasks were repeated randomly under different condi-  
 596 tions, depending on the display type and the tracing metaphor for  
 597 a total of 8 tasks (see Fig. 9). Between each task a break of five



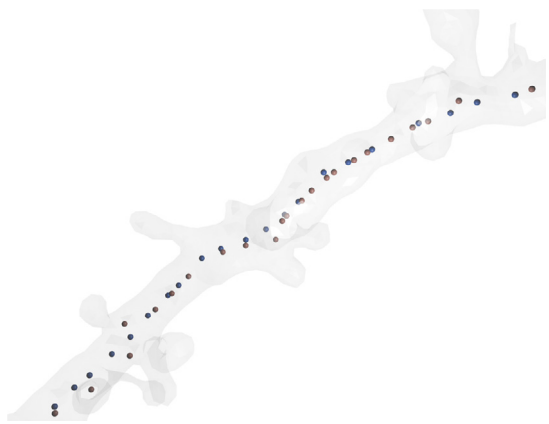
**Fig. 9. User study protocol:** subjects were asked to perform eight skeleton editing tasks under different conditions related to tracing metaphor and display setups.



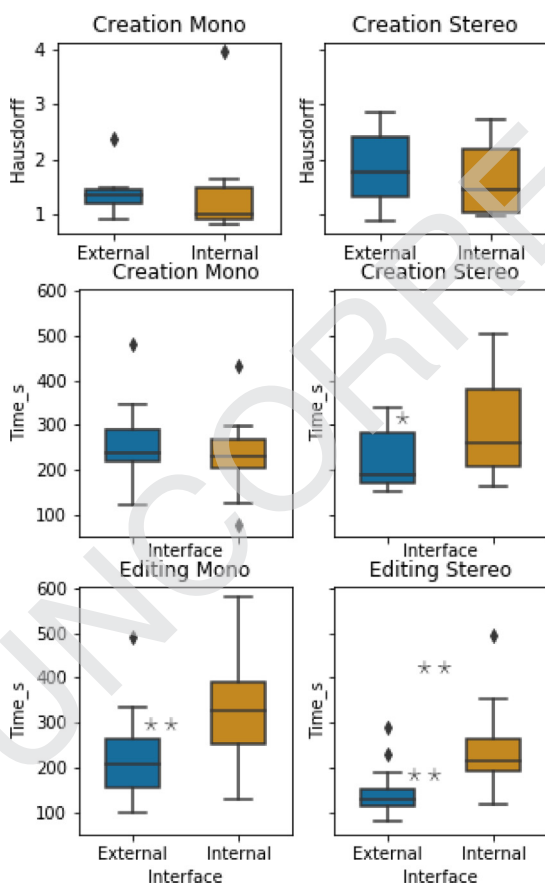
**Fig. 10. User study data:** subjects were asked to perform eight editing tasks under different conditions on two long processes from Neuron1 (left) and Neuron2 (right).

598 minutes was given to subjects. After one task was complete (un-  
 599 der the 4 conditions), users were asked to fill a 6 questions NASA-  
 600 TLX form for comparing mental demand, physical demand, tempo-  
 601 ral demand, performance, effort and frustration (see Table 6), with  
 602 a 5 value Likert scale score ranging from low to high [57]. During  
 603 the tasks we measured the total time for performing the tasks, and  
 604 the paths of the traced branch. The tests were designed in a way  
 605 that users did not need more than 60 min for training, completing  
 606 all tasks, and filling the forms. Think-out-loud comments were also  
 607 recorded during sessions.

608 *Quantitative performance.* For measuring performance in crea-  
 609 tion and editing tasks we compared branches obtained by users  
 610 with respect to ground truth obtained by MCS [27]. Fig. 11 shows  
 611 an example of a branch created by a user (in pink), and the cor-  
 612 responding ground truth (in blue). Fig. 12 shows performance re-  
 613 sults for the tests related to accuracy for trace branches and the  
 614 completion time, obtained after filtering very few outliers of sub-  
 615 jects exhibiting really poor performance. We show results in form  
 616 of boxplots: the bottom and top of each box are the first and



**Fig. 11. Accuracy measurement.** We measure the accuracy of branch creation through Hausdorff distance between the ground truth branch computed by MCS [27] (in blue in this example), and the branch traced by subjects (in pink in this example). (For interpretation of the references to color in this figure legend, the reader is referred to the web version of this article.)



**Fig. 12. Quantitative performance.** Boxplots of accuracy performance for creation task (Hausdorff distance with respect to ground truth computed with Mean Curvature Flow in top row), and time performance for creation task (middle row) and editing task (bottom row). The bottom and top of each box are the first and third quartiles, the black line inside the box is the second quartile (the median), and the ends of the whiskers extending vertically from the boxes represent the lowest datum still within 1.5 IQR (inter-quartile range) of the lower quartile, and the highest datum still within 1.5 IQR of the upper quartile.

third quartiles, the black line inside the box is the second quartile (the median), and the ends of the whiskers extending vertically from the boxes represent the lowest datum still within 1.5 IQR (inter-quartile range) of the lower quartile, and the highest datum still within 1.5 IQR of the upper quartile. Outliers are indicated as small circles. On top we show the accuracy of tracing in form of Hausdorff distance in  $\mu m$  between the branch created by subjects and the ground-truth branch computed through Mean Curvature Flow [27]: given two point sets  $\mathbf{X}$ ,  $\mathbf{Y}$  representing two branches, we measure the symmetric Hausdorff distance [58] as the maximum of the asymmetric directed Hausdorff distance  $H(\mathbf{X}, \mathbf{Y}) = \max(\hat{H}(\mathbf{X}, \mathbf{Y}), \hat{H}(\mathbf{Y}, \mathbf{X}))$ , where the directed Hausdorff distance is defined as

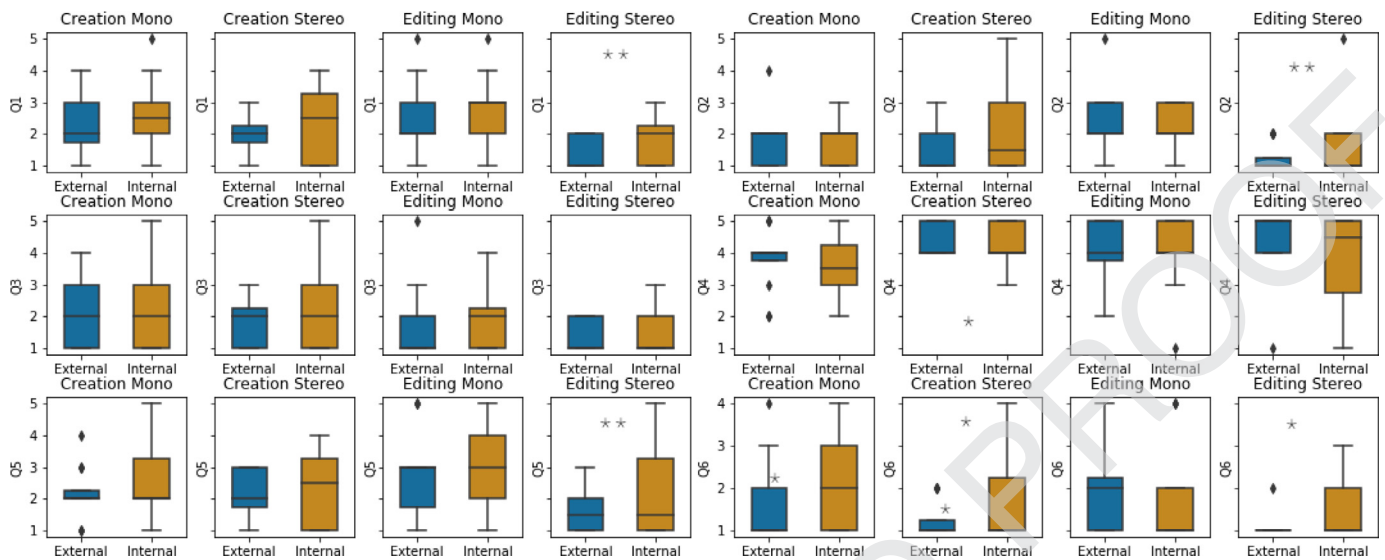
$$\hat{H}(\mathbf{X}, \mathbf{Y}) = \max_{x \in \mathbf{X}} (\min_{y \in \mathbf{Y}} \|x - y\|). \quad (1)$$

ANOVA on the Hausdorff distance showed no effects due to the display for accuracy ( $1.49 \pm 0.88$  with Mono setup versus  $1.74 \pm 0.72$  with Stereo setup). Also the different interfaces do not appear to affect accuracy ( $1.63 \pm 0.65$  with External interface versus  $1.60 \pm 0.96$  with the Internal interface). On the bottom we compare the task completion time, either for the creation process (middle row) and the editing process (bottom row). ANOVA revealed an effect on interface when used with Stereo setup ( $p = .06$  with  $F = 3.893314$ ) for the creation task, with  $T = 218 \pm 64.6s$  for external interface, and  $T = 292 \pm 117.7 s$  for internal interface, indicating that the external interface appears to be faster for creation especially in VR setup. Moreover, ANOVA revealed an important effect for editing either related to the display setup ( $p = .007$  with  $F = 8.106935$ ) and the interface ( $p = .001$  for  $F = 12.24$ ), indicating that external interface is perceived more comfortable and users perform editing tasks faster when they use the VR setup.

**Qualitative performance.** Table 6 shows the questions and results of NASA-TLX questionnaire proposed to subjects after tasks in order to evaluate their perception of performance, satisfaction, fatigue and stress under the different conditions.

Fig. 13 shows the boxplots of answers on a Likert scale (1=low,5=high). ANOVA on answers revealed a slight effect for satisfaction during the tracing task due to display setup ( $p = .03$  and  $F = 5.29$  for question Q4 in favor of VR setup), and effects on stress of display ( $p = .1$  and  $F = 2.81$  for question Q6 in favor of VR setup), and interface ( $F = 3.93$  and  $p = .05$  for question Q6 in favor of external tracing). With respect to the editing task, ANOVA revealed significant effects related to the display for mental demand ( $F = 12.67$  and  $p = .001$  for question Q1 in favor of VR setup), physical demand ( $F = 12.86$  and  $p = .0008$  for question Q2 in favor of VR setup), fatigue ( $F = 8.14$  and  $p = .006$  for question Q5 in favor of VR setup), and stress ( $f = 3.32$  and  $p = .07$  for question Q6 in favor of VR setup). No significant effects were found due to the different editing interface.

**Discussion.** By observing the behavior of users with the system, we could note that the learning curve was rapid and the process per-se was pretty straight forward. In general, while performing the tasks, all operations required some time for the user to learn how to switch from one function to another one. To note also in this case the learning curve was pretty fast for experienced tracers. For the usage of the system on display wall setup, we realized that it is a factor of advantage if the user is a gamer, when using the XBOX controller: expert gamers appeared to be more comfortable and to navigate blindly and effortlessly. In general the user study revealed that subjects feel more in control when in VR, since the orientation, navigation and interaction is more natural, and they can contribute with body, head and hands and not just two joysticks that restrict movement, eyesight and perspective. Since we



**Fig. 13. Qualitative evaluation.** Boxplots of answers in Likert scale for questions in Table 6 for two different editing metaphors (external and internal), two different setups (Mono and Stereo), and two different tasks (creating and editing). The bottom and top of each box are the first and third quartiles, the black line inside the box is the second quartile (the median), and the ends of the whiskers extending vertically from the boxes represent the lowest datum still within 1.5 IQR (inter-quartile range) of the lower quartile, and the highest datum still within 1.5 IQR of the upper quartile.

**Table 6**

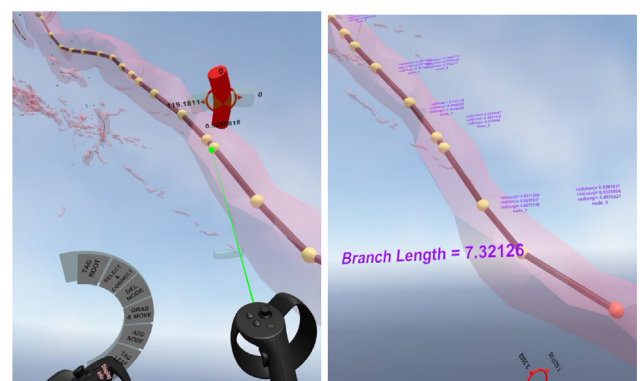
**User evaluation:** 12 subjects were asked to compare two different editing metaphors (external and internal) on two different setups (Mono and Stereo) for two different tasks (creating and editing). Table shows the results of the answers of a 6-item questionnaire [?] on a Likert scale (1=low,5=high).

| Question                             | Results (Likert scale: 1=low 5=high) |           |           |           |           |           |           |           |
|--------------------------------------|--------------------------------------|-----------|-----------|-----------|-----------|-----------|-----------|-----------|
|                                      | Creation                             |           |           |           | Editing   |           |           |           |
|                                      | Stereo                               |           | Mono      |           | Stereo    |           | Mono      |           |
|                                      | External                             | Internal  | External  | Internal  | External  | Internal  | External  | Internal  |
| Q1: How mentally demanding was it?   | 2.0 ± 0.7                            | 2.4 ± 1.2 | 2.2 ± 0.9 | 2.7 ± 1.1 | 1.4 ± 0.5 | 1.8 ± 0.8 | 2.5 ± 1.1 | 2.7 ± 1.2 |
| Q2: How physically demanding was it? | 1.4 ± 0.7                            | 2.0 ± 1.3 | 1.8 ± 0.9 | 1.7 ± 0.7 | 1.3 ± 0.5 | 1.6 ± 1.2 | 2.3 ± 1.1 | 2.3 ± 0.7 |
| Q3: How hurried was the pace?        | 1.9 ± 0.8                            | 2.2 ± 1.3 | 2.1 ± 1.2 | 2.3 ± 1.3 | 1.3 ± 0.5 | 1.5 ± 0.8 | 1.8 ± 1.2 | 1.9 ± 1.0 |
| Q4: How successful were you?         | 4.3 ± 0.5                            | 4.2 ± 0.7 | 3.8 ± 1.0 | 3.7 ± 1.0 | 4.4 ± 1.2 | 3.8 ± 1.5 | 3.9 ± 1.1 | 4.0 ± 1.1 |
| Q5: How hard did you have to work ?  | 2.1 ± 0.8                            | 2.3 ± 1.3 | 2.2 ± 0.8 | 2.7 ± 1.2 | 1.6 ± 0.7 | 2.2 ± 1.5 | 2.8 ± 1.4 | 3.0 ± 1.2 |
| Q6: How stressed were you?           | 1.3 ± 0.5                            | 1.7 ± 1.1 | 1.7 ± 1.0 | 2.3 ± 1.1 | 1.1 ± 0.3 | 1.6 ± 0.8 | 1.9 ± 1.0 | 1.7 ± 1.2 |

679 designed the duration of tests in a way to do not let subjects per-  
 680 ceive any problem of cybersickness (maximum 10 minutes for each  
 681 task, and 5 minutes break between the tasks), results of the user  
 682 study appear to be in contradiction with respect to the evaluation  
 683 performed by expert users during the tracing of entire cells. It was  
 684 a conscious decision during the design of the user study, even if  
 685 we are aware that it would be important to evaluate the effects of  
 686 cybersickness and to find ways to reduce it. We plan to carry out  
 687 further user study investigations in future, with different task du-  
 688 ration, in order to better evaluate the effects of cybersickness and  
 689 physical efforts on our framework.

690 **7.3. Case study: Analysis of branch-based intracellular organelles.**

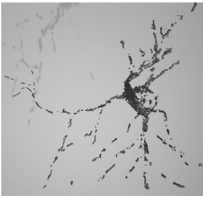
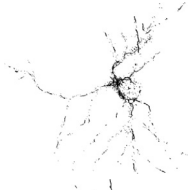


691 One of the significant benefits of having skeleton representa-  
 692 tions of brain cells is the possibility of computing accurate mea-  
 693 surements of morphological features. As a preliminary test, neuro-  
 694 scientists performed analysis of mitochondria, which are intracel-  
 695 lular structures within the neural cells Neuron1 and Neuron2 (see  
 696 Table 7). Since scientists are particularly interested in measuring  
 697 specific geometric features of organelles, like lengths and radii  
 698 (maximum, minimum, and average), adequate skeleton representa-  
 699 tions are needed for performing accurate measures. To this end,  
 700 our system uses the same functionality equipped in the VR path  
 701 stabilizer. Users can point at a particular node from a branch of



**Fig. 14. Branch-based measurements.** Our system performs calculations of measurements on intracellular structures. Left: User points the laser pointer at any node of a branch of interest to display node-relevant measurements. Right: Measurements of a mitochondrion branch are displayed.

interest, and the system uses the skeleton information for provid-  
 ing the measure of the full length, along with the radius values  
 at each skeletal node contained in that branch. The measured val-  
 ues are shown as text labels in the scene on top of each node and  
 recorded for subsequent statistical analysis (see Fig. 14).

**Table 7**  
The intracellular structures of Neuron1 and Neuron2 showing mitochondria morphology, side by side with their skeletons generated via the MCS algorithm.

| Cell Name    | Morphology  | MC Skeleton  | Nodes  Edges  Branches |
|--------------|---|--|------------------------|
| Mito Neuron1 |  |  | 2246  1963  1396       |
| Mito Neuron2 |  |  | 1749  1656  811        |

## 707 8. Conclusion

708 We presented an immersive system for creating, proofreading  
709 and exploring medial axis representations from highly detailed  
710 brain cellular morphologies reconstructed from serial electron mi-  
711 croscopy. The framework is designed for stereoscopic HMD dis-  
712 play setups and extended to large-scale monocular displays in a  
713 way to alleviate unpleasant side-effects like cyber-sickness and fa-  
714 tigue, while still providing the ability to edit the skeleton in an  
715 immersive way. The system is currently used by neuroscientists  
716 for deriving accurate skeleton representations to be used for clas-  
717 sification, measurements, and simulation purposes [8]. We pre-  
718 sented the outcomes of a user study to evaluate and compare the  
719 strengths the proposed system.

720 Our subjective preliminary evaluation showed that domain sci-  
721 entists feel particularly comfortable in using the system for proof-  
722 reading and editing previously computed skeletons while they still  
723 consider the process of creating medial axis representations from  
724 scratch to be comparable to automated or semi-automated 3D  
725 tools, in terms of time consumption, although they recognised how  
726 powerful the path stabilizer approach is to find the medial axis  
727 automatically, and the combination of external and internal trac-  
728 ing metaphors dramatically speed-up the creation process. Plans  
729 to improve the system include the implementation of online col-  
730 laborative schemes, in order to distribute the creation process  
731 among multiple users, reduce the working time and effort, and  
732 at the same time increase the quality of the output representa-  
733 tion; and integration of visual analytics tools for exploring feature  
734 distributions inside morphologies [59] and tools for performing vi-  
735 sual analysis of topological data representations associated to me-  
736 dial axis representations [40]. Finally we customized the system  
737 for two different setups, considering direct metric interaction, and  
738 standard gaming indirect interfaces [54]. We did not yet investi-  
739 gate alternative interfaces that could speed-up the editing process  
740 and exploration, like touch-based systems to be attached to the  
741 display wall setup or gesture recognition systems to be attached  
742 to the stereoscopic HMD setup. We plan to explore this avenue, in  
743 order to understand which interface is more performing for these  
744 kind of neuroscience investigations.

## 745 Declaration of Competing Interest

746 The authors declare that they have no known competing finan-  
747 cial interests or personal relationships that could have appeared to  
748 influence the work reported in this paper.

## CRediT authorship contribution statement

**Daniya Boges:** Methodology, Formal analysis. **Marco Agus:** Methodology, Formal analysis, Supervision, Writing - original draft, Writing - review & editing. **Ronell Sicut:** Methodology, Supervision, Validation. **Pierre J. Magistretti:** Funding acquisition, Investigation, Formal analysis. **Markus Hadwiger:** Methodology, Supervision, Writing - review & editing. **Corrado Cali:** Project administration, Data curation, Methodology, Writing - review & editing.

## Acknowledgment

This work is supported by KAUST King Abdullah University of Science and Technology KAUST-EPFL Alliance for Integrative Modeling of Brain Energy Metabolism <https://www.kaust.edu.sa/en> under KAUST CRG6 Grant No. 2313. We thank all the participants of the user study from KAUST and from the Neuroscience Institute "Cavaliere Ottolenghi". We also thank the anonymous reviewers for useful comments and suggestions.

## Supplementary material

Supplementary material associated with this article can be found, in the online version, at doi:[10.1016/j.cag.2020.05.024](https://doi.org/10.1016/j.cag.2020.05.024)

## References

- [1] Cali C, Agus M, Kare K, Boges D, Lehvälaiho H, Hadwiger M, et al. 3D cellular reconstruction of cortical glia and parenchymal morphometric analysis from serial block-face electron microscopy of juvenile rat. *Prog Neurobiol* 2019. In press
- [2] Coggan JS, Keller D, Cali C, Lehvälaiho H, Markram H, Schürmann F, et al. Norepinephrine stimulates glycogenolysis in astrocytes to fuel neurons with lactate. *PLoS Comput Biol* 2018;14(8):e1006392.
- [3] Markram H, Muller E, Ramaswamy S, Reimann M, Abdellah M, Sanchez C, et al. Reconstruction and simulation of neocortical microcircuitry. *Cell* 2015;163(2):456–92. doi:[10.1016/j.cell.2015.09.029](https://doi.org/10.1016/j.cell.2015.09.029).
- [4] Cali C, Baghabra J, Boges DJ, Holst GR, Kreshuk A, Hamprecht FA, et al. Three-dimensional immersive virtual reality for studying cellular compartments in 3d models from EM preparations of neural tissues: 3d virtual reality for neural tissue. *J Comp Neurol* 2016;524(1):23–38. doi:[10.1002/cne.23852](https://doi.org/10.1002/cne.23852).
- [5] Agus M, Boges D, Gagnon N, Magistretti PJ, Hadwiger M, Cali C. Glam: glycogen-derived lactate absorption map for visual analysis of dense and sparse surface reconstructions of rodent brain structures on desktop systems and virtual environments. *Comput Graph* 2018;74:85–98.
- [6] Usher W, Klacansky P, Federer F, Bremer P-T, Knoll A, Yarch J, et al. A virtual reality visualization tool for neuron tracing. *IEEE Trans Vis Comput Graph* 2017;24(1):994–1003.
- [7] Vezzoli E, Cali C, De Roo M, Ponzoni L, Sogne E, Gagnon N, et al. Ultrastructural evidence for a role of astrocytes and glycogen-derived lactate in learning-dependent synaptic stabilization. *Cerebral Cortex* 2019.

- 793 [8] Kanari L, Ramaswamy S, Shi Y, Morand S, Meystre J, Perin R, et al. Objective  
794 morphological classification of neocortical pyramidal cells. *Cerebral Cortex*  
795 2019;29(4):1719–35. doi:10.1093/cercor/bhy339.
- 796 [9] Longair MH, Baker DA, Armstrong JD. Simple neurite tracer: open source  
797 software for reconstruction and analysis of neuronal processes. *Bioinformatics*  
798 2011;27(17):2453–4.
- 799 [10] Schindelin J, Arganda-Carreras I, Frise E, Kaynig V, Longair M, Pietzsch T,  
800 et al. Fiji: an open-source platform for biological-image analysis. *Nat Methods*  
801 2012;9(7):676.
- 802 [11] Schindelin J, Rueden CT, Hiner MC, Eliceiri KW. The image ecosystem: an open  
803 platform for biomedical image analysis. *Mol Reprod Dev* 2015;82(7–8):518–29.
- 804 [12] Tagliasacchi A, Delame T, Spagnuolo M, Amenta N, Telea A. 3d skeletons: A  
805 state-of-the-art report. In: Proceedings of the 37th Annual Conference of the  
806 European Association for Computer Graphics: State of the Art Reports. Goslar  
807 Germany, Germany: Eurographics Association; 2016. p. 573–97. doi:10.1111/cgf.  
808 12865.
- 809 [13] Boges D, Cal C, Magistretti PJ, Hadwiger M, Sicut R, Agus M. Immersive En-  
810 vironment for Creating, Proofreading, and Exploring Skeletons of Nanometric  
811 Scale Neural Structures. *Smart Tools and Apps for Graphics - Eurographics Italian*  
812 *Chapter Conference*. Agus M, Corsini M, Pintos R, editors. The Eurographics  
813 Association; 2019. ISBN 978-3-03868-100-7. doi:10.2312/stag.20191360.
- 814 [14] Mohammed H, Al-Awami A, Beyer J, Cali C, Magistretti PJ, Pfister H, et al. Ab-  
815 stractocyte: a visual tool for exploring nanoscale astroglial cell morphology. *PacificVis*;  
816 2017.
- 817 [15] Hadwiger M, Al-Awami A, Beyer J, Agus M, Pfister H. SparseLeap: Efficient  
818 Empty Space Skipping for Large-Scale Volume Rendering. 2017.
- 819 [16] Keiriz J, Zhan L, Chukhman M, Ajilore O, Leow A.D., Forbes A.G. Exploring  
820 the human connectome topology in group studies. arXiv preprint  
821 arXiv:1706102972017..
- 822 [17] Agus M, Gobbetti E, Iglesias Guitián JA, Marton F. Evaluating layout discrim-  
823 ination capabilities of continuous and discrete automultiscopic displays. In:  
824 Proc. Fourth International Symposium on 3D Data Processing, Visualization and  
825 Transmission; 2010.
- 826 [18] Hänel C, Pieperhoff P, Hentschel B, Amunts K, Kuhlen T. Interactive 3d visu-  
827 alization of structural changes in the brain of a person with corticobasal syn-  
828 drome. *Front Neuroinform* 2014;8:42.
- 829 [19] Laha B, Sensharma K, Schiffbauer JD, Bowman DA. Effects of immersion on  
830 visual analysis of volume data. *IEEE Trans Vis Comput Graph* 2012;18(4):597–  
831 606.
- 832 [20] Agus M, Gobbetti E, Iglesias Guitián J, Marton F, Pintore G. Gpu accelerated  
833 direct volume rendering on an interactive light field display. *Comput Graphics*  
834 *Forum* 2008;27(3):231–40. *Proc. Eurographics 2008*
- 835 [21] Laha B, Bowman DA, Socha JJ. Effects of vr system fidelity on analyzing  
836 isosurface visualization of volume datasets. *IEEE Trans Vis Comput Graph*  
837 2014;20(4):513–22.
- 838 [22] Forsberg A, Katzourin M, Wharton K, Slater M, et al. A comparative study of  
839 desktop, fishtank, and cave systems for the exploration of volume rendered  
840 confocal data sets. *IEEE Trans Vis Comput Graph* 2008;14(3):551–63.
- 841 [23] Alper B, Hollerer T, Kuchera-Morin J, Forbes A. Stereoscopic highlighting:  
842 2d graph visualization on stereo displays. *IEEE Trans Vis Comput Graph*  
843 2011;17(12):2325–33.
- 844 [24] Arsiwalla XD, Zucca R, Betella A, Martinez E, Dalmazzo D, Omedas P, et al.  
845 Network dynamics with brainx3: a large-scale simulation of the human brain  
846 network with real-time interaction. *Front Neuroinform* 2015;9:2.
- 847 [25] Xu R, Thomas MM, Leow A, Ajilore OA, Forbes AG. Tempocave: Visualizing dy-  
848 namic connectome datasets to support cognitive behavioral therapy. In: 2019  
849 IEEE Visualization Conference (VIS). IEEE; 2019. p. 186–90.
- 850 [26] Sobiecki A, Jalba A, Telea A. Comparison of curve and surface skeletonization  
851 methods for voxel shapes. *Pattern Recogn Lett* 2014;47:147–56. doi:10.1016/j.  
852 patrec.2014.01.012.
- 853 [27] Tagliasacchi A, Alhashim I, Olson M, Zhang H. Mean curvature skeletons. *Comput*  
854 *Graph Forum* 2012;31(5):1735–44. doi:10.1111/j.1467-8659.2012.03178.x.
- 855 [28] Yan Y, Sykes K, Chambers E, Letscher D, Ju T. Erosion thickness on medial axes  
856 of 3d shapes. *ACM Trans Graph* 2016;35(4):38:1–38:12. doi:10.1145/2897824.  
857 2925938.
- 858 [29] Livesu M, Attene M, Patané G, Spagnuolo M. Explicit cylindrical maps for gen-  
859 eral tubular shapes. *Comput-Aided Des* 2017;90:27–36.
- 860 [30] Li P, Wang B, Sun F, Guo X, Zhang C, Wang W. Q-Mat: computing medial axis  
861 transform by quadratic error minimization. *ACM Trans Graph* 2015;35(1):8:1–  
862 8:16. doi:10.1145/2753755.
- 863 [31] Yan Y, Letscher D, Ju T. Voxel cores: efficient, robust, and provably good  
864 approximation of 3d medial axes. *ACM Trans Graph* 2018;37(4):44:1–44:13.  
865 doi:10.1145/3197517.3201396.
- 866 [32] Sato M, Bitter I, Bender MA, Kaufman AE, Nakajima M. Teasar: Tree-structure  
867 extraction algorithm for accurate and robust skeletons. In: Proceedings of the  
868 8th pacific conference on computer graphics and applications. Washington, DC,  
869 USA: IEEE Computer Society; 2000 <http://dl.acm.org/citation.cfm?id=826029.826514>. ISBN 0-7695-0868-5. 281–
- 870 [33] Westenberger P. Avizo-3d visualization framework. In: *Geoinformatics confer-*  
871 *ence*; 2008. p. 1–11.
- 872 [34] Gillette TA, Ascoli GA. Topological characterization of neuronal arbor mor-  
873 phology via sequence representation: l-motif analysis. *BMC Bioinformatics*  
874 2015;16(1):216.
- 875 [35] Gillette TA, Hosseini P, Ascoli GA. Topological characterization of neuronal ar-  
876 bor morphology via sequence representation: ii-global alignment. *BMC Bioin-*  
877 *form* 2015;16(1):209.
- 878 [36] Li Y, Wang D, Ascoli GA, Mitra P, Wang Y. Metrics for comparing neuronal tree  
879 shapes based on persistent homology. *PLoS One* 2017;12(8):e0182184.
- 880 [37] Batabyal T, Acton ST. Neurosol: automated classification of neurons using the  
881 sorted laplacian of a graph. In: 2017 IEEE 14th international symposium on  
882 biomedical imaging (ISBI 2017). IEEE; 2017. p. 397–400.
- 883 [38] Batabyal T, Acton ST. Elastic path2path: automated morphological classifica-  
884 tion of neurons by elastic path matching. In: 2018 25th IEEE international  
885 conference on image processing (ICIP); 2018. p. 166–70. doi:10.1109/ICIP.2018.  
886 8451446.
- 887 [39] Riihimäki H., Chacholski W., Theorell J., Hillert J., Ramanujam R. A topologi-  
888 cal data analysis based classification method for multiple measurements. arXiv  
889 preprint arXiv:1904029712019..
- 890 [40] Kanari L, Dlotko P, Scolamiero M, Levi R, Shillcock J, Hess K, et al. A topo-  
891 logical representation of branching neuronal morphologies. *Neuroinformatics*  
892 2018;16(1):3–13. doi:10.1007/s12021-017-9341-1.
- 893 [41] Abdellah M, Hernando J, Eilemann S, Lapere S, Antille N, Markram H, et al.  
894 Neuromorphovis: a collaborative framework for analysis and visualization of  
895 neuronal morphology skeletons reconstructed from microscopy stacks. *Bioin-*  
896 *formatics* 2018;34(13):i574–82.
- 897 [42] Titze B, Genoud C. Volume scanning electron microscopy for imaging biological  
898 ultrastructure. *Biol Cell* 2016;108(11):307–23. doi:10.1111/boc.201600024.
- 899 [43] Lichtman JW, Pfister H, Shavit N. The big data challenges of connectomics. *Nat*  
900 *Neurosci* 2014;17(11):1448–54.
- 901 [44] Coggan JS, Cali C, Keller D, Agus M, Boges D, Abdellah M, et al. A pro-  
902 cess for digitizing and simulating biologically realistic oligocellular networks  
903 demonstrated for the neuro-glio-vascular ensemble. *Front Neurosci* 2018;12.  
904 doi:10.3389/fnins.2018.00664.
- 905 [45] Sommer C, Straehle C, Köthe U, Hamprecht FA. Ilastik: Interactive learning  
906 and segmentation toolkit. In: 2011 IEEE international symposium on biomedical  
907 imaging: From nano to macro. IEEE; 2011. p. 230–3. doi:10.1109/ISBI.2011.  
908 5872394.
- 909 [46] Cardona A, Saalfeld S, Schindelin J, Arganda-Carreras I, Preibisch S, Long-  
910 air M, et al. Trakem2 software for neural circuit reconstruction. *PLoS One*  
911 2012;7(6):e38011. doi:10.1371/journal.pone.0038011.
- 912 [47] Agus M, Cali C, Al-Awami A, Gobbetti E, Magistretti P, Hadwiger M. Interactive  
913 volumetric visualization of glycogen-derived energy absorption in nanometric  
914 brain structures. *Comput Graph Forum* 2019;38(3):427–39.
- 915 [48] Murray JW. Building virtual reality with unity and steam VR. AK Peters/CRC  
916 Press; 2017.
- 917 [49] Desai P.R., Desai P.N., Ajmera K.D., Mehta K.A. A review paper on oculus rift-a  
918 virtual reality headset. arXiv preprint arXiv:14081172014.
- 919 [50] Dempsey P. The teardown: htc vive vr headset. *Eng Technol* 2016;11(7–8):80–  
920 1.
- 921 [51] Hess R. The essential blender: guide to 3D creation with the open source suite  
922 blender. No Starch Press; 2007.
- 923 [52] Cignoni P, Callieri M, Corsini M, Dellepiane M, Ganovelli F, Ranzuglia G. Mesh-  
924 lab: an open-source mesh processing tool. In: *Eurographics Italian chapter*  
925 *conference*, 2008; 2008. p. 129–36.
- 926 [53] Maraj C, Hurter J, Ferrante S, Horde L, Carter J, Murphy S. Oculus rift versus  
927 htc vive: usability assessment from a teleoperation task. In: *International con-*  
928 *ference on human-computer interaction*. Springer; 2019. p. 247–57.
- 929 [54] Mendes D, Caputo FM, Giachetti A, Ferreira A, Jorge J. A survey on 3d virtual  
930 object manipulation: from the desktop to immersive virtual environments. In:  
931 *Computer graphics forum*, 38. Wiley Online Library; 2019. p. 21–45.
- 932 [55] Cali C, Baghabra J, Boges DJ, Holst GR, Kreshuk A, Hamprecht FA, et al. 3D  
933 immersive virtual reality for studying cellular compartments in 3D models from  
934 EM preparations of neural tissues. *J Comp Neurol* 2016;524(1):23–38.
- 935 [56] Jaeger S, Klein K, Joos L, Zagermann J, de Ridder M, Kim J, et al. Challenges  
936 for brain data analysis in vr environments. In: 2019 IEEE pacific visualization  
937 symposium (PacificVis). IEEE; 2019. p. 42–6.
- 938 [57] Hart SG. Nasa-task load index (nasa-tlx); 20 years later. In: *Proceedings of the*  
939 *human factors and ergonomics society annual meeting*, 50. Sage Publications  
940 Sage CA: Los Angeles, CA; 2006. p. 904–8.
- 941 [58] Taha AA, Hanbury A. An efficient algorithm for calculating the exact hausdorff  
942 distance. *IEEE Trans Pattern Anal Mach Intell* 2015;37(11):2153–63.
- 943 [59] Sicut R, Li J, Choi J, Cordeil M, Jeong W-K, Bach B, et al. Dxr: a toolkit  
944 for building immersive data visualizations. *IEEE Trans Vis Comput Graph*  
945 2018;25(1):715–25.